THE GEOLOGICAL SOCIETY OF AMERICA®

New age and lake chemistry constraints on the Aptian pre-salt carbonates of the central South Atlantic

M. Lawson[1,†], J. Sitgreaves[2], T. Rasbury[3], K. Wooton[3], W. Esch[2], V. Marcon[2], S. Henares[2], A. Konstantinou[2], E. Kneller[2], D. Gombosi[2], V. Torres[2], A. Silva[4], R. Alevato[4], M. Wren[2], S. Becker[2], and J. Eiler[5]

[1]*Aker BP, Stavanger 4020, Norway*
[2]*ExxonMobil, Springwoods Village Parkway, Spring, Texas 77027, USA*
[3]*Department of Geosciences, Stony Brook University, Stony Brook, New York 11794, USA*
[4]*ExxonMobil Exploração Brasil, Rua Lauro Muller, Rio de Janeiro, Rio de Janeiro 22290-160, Brazil*
[5]*Division of Geological and Planetary Sciences, California Institute of Technology, East California Boulevard, Pasadena, California 91125, USA*

ABSTRACT

The Cretaceous lacustrine carbonates of the offshore Brazilian and West African pre-salt basins represent some of the most extensive non-marine carbonates discovered in the geologic record. Despite being intensively studied over the past decade, the age of these carbonates and the overlying regional salt sequences is highly controversial. Similarly, the conditions under which these carbonates were deposited remains poorly understood. Here, we provide the first integrated geochronology-thermometry study of these carbonates to develop an improved understanding of when and under what conditions they formed. We utilize carbonate clumped isotope and $^{87}Sr/^{86}Sr$ geochemistry alongside traditional petrographic techniques to identify samples minimally altered from burial diagenesis that may yield reliable age and lake chemistry constraints. Carbonate clumped isotope apparent temperatures for the studied carbonates range from 36 °C to 91 °C, which we infer to represent a range in sample preservation from minimally altered depositional temperatures through to those that have been overprinted by burial diagenesis. $^{87}Sr/^{86}Sr$ values of our samples are consistent with those of previous studies for Cretaceous pre-salt carbonates that have not experienced significant alteration from hydrothermal fluids. Through this approach, we measured the first high resolution isotope dilution U-Pb age constraint of 115.83 ± 1.56 Ma (2σ) on a well preserved carbonate. Combined with overlapping lower resolution laser ablation U-Pb ages for time-equivalent stratigraphy on two separate carbonate platforms of 114.46 ± 4.72 Ma and 109.73 ± 9.26 Ma, these ages provide the first robust direct age calibration for pre-salt carbonates deposited on either side of the South Atlantic during the final stages of the break-up of Gondwana in the Early Cretaceous. These ages also provide the first calibration for a combined $^{87}Sr/^{86}Sr$-facies-log based relative age framework within the Santos Basin, offshore Brazil. We further utilize $\delta^{18}O$ constraints on samples that yield depositional clumped isotope apparent temperatures to constrain the $\delta^{18}O$ of the water in these ancient lakes to between 1.9 and 4.9‰$_{\text{Vienna standard mean ocean water}}$. Such heavy values reveal a picture of a hot and arid environment. This is consistent with prior biostratigraphic studies of the carbonates that show a decrease in faunal diversity in these lakes prior to marine ingress and the development of open marine conditions in the South Atlantic Ocean.

INTRODUCTION

The Early Cretaceous breakup of Gondwana created basins offshore Brazil with conjugates in West Africa (Fig. 1). A key feature of these basins is the presence of one of the most regionally expansive salt sequences in the geologic record, occurring in the final stages of continental break-up, and extending ~2200 km from the Sergipe Basin in the north to the Santos Basin in the south (Szatmari et al., 2021). Until recently, these evaporites masked the full extent of the pre-salt geologic archive and the important regional temporal and environmental conditions it records of the terminal stages of continental break-up and early seafloor spreading. Following improvements in seismic imaging over the past decade and calibration from exploration drilling, a picture is emerging of a vast lake system that produced extensive lacustrine carbonates prior to the development of open marine conditions in the South Atlantic Ocean. Indeed, the Barra Velha Formation (Fm) carbonate reservoirs of the Santos Basin form part of the largest lacustrine carbonate system discovered in the Phanerozoic record (Wright, 2022).

One of the main challenges in developing a robust understanding of these basins is the total absence of reliable time markers to place any environmental constraints into temporal context. This has led to significant uncertainty on the age of key sequences within the stratigraphy. The Ariri Fm that represents the Santos Basin equivalent of the regional evaporite sequence, for example, has been proposed to be as young as 111 Ma based on an Ar-Ar age of sylvinite of 110.64 ± 0.3 Ma from the Sergipe Basin (Szatmari et al., 2021). Further, evaporites unconformably overly volcanic rocks dated at 113.2 ± 0.1 Ma in the northern Pelotas Basin (Davison, 2007; Dias et al., 1994). However, biostratigraphic data from the Deep Sea Drilling Project Site 364 (offshore Angola) suggest that the first marine deposition above these evaporites occurred during the late Aptian prior to 113 Ma (Kochhann et al., 2013). This has been further supported by the study of Sanjinés et al. (2022), who also report upper Aptian aged fauna in the stratigraphy immediately overlying the evaporites in numerous wells within the

M. Lawson https://orcid.org/0000-0003-2743-3773
†Previous address: ExxonMobil, Springwoods Village Parkway, Spring, Texas 77027, USA; miclawson@gmail.com.

GSA Bulletin;
published online 8 June 2022

https://doi.org/10.1130/B36378.1; 7 figures; 2 tables; 1 supplemental file.

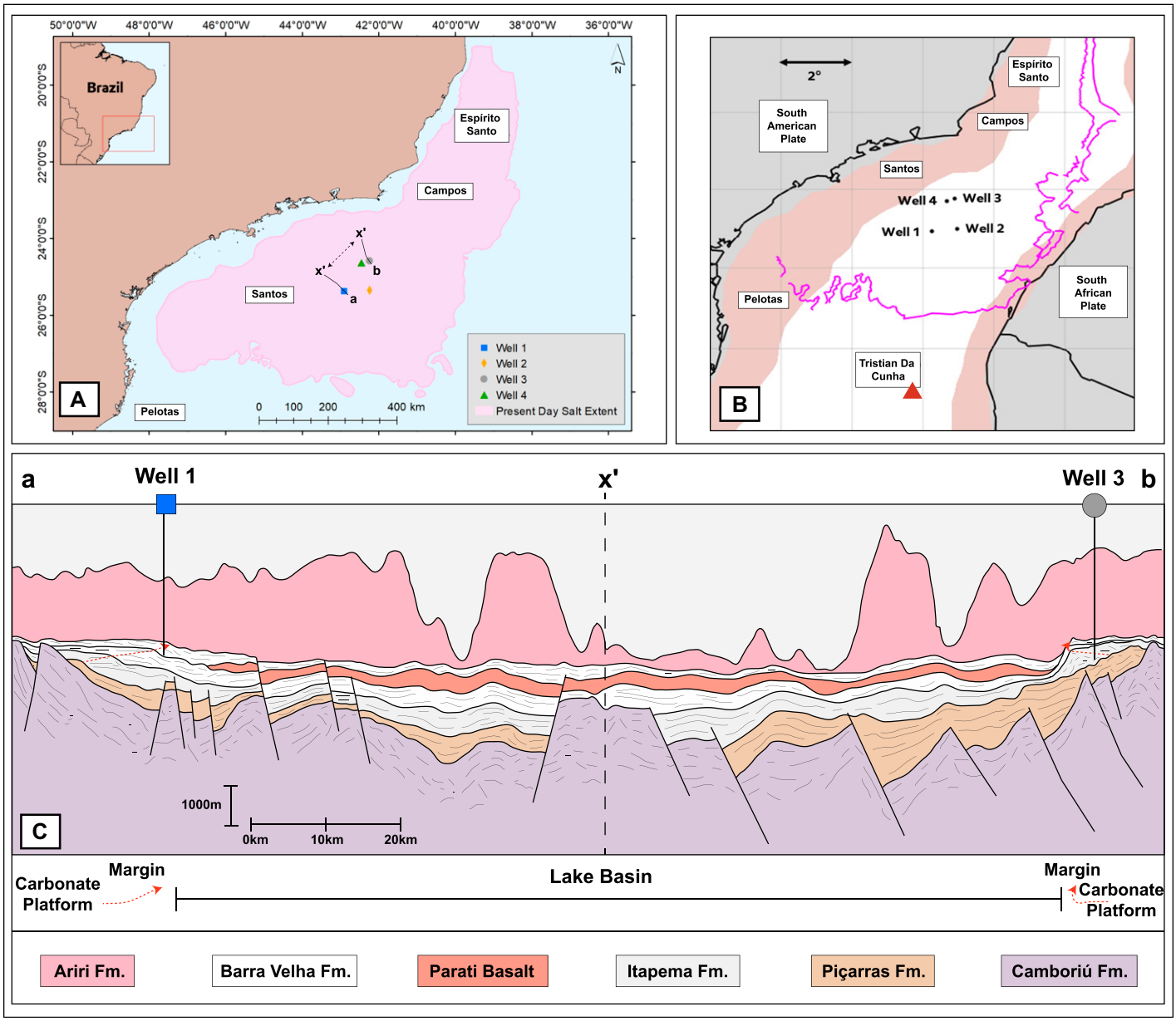

Figure 1. (A) Well locations in the Santos Basin, offshore Brazil, relative to the full extent of the Brazil salt basins. (B) Reconstructed basement at 115 Ma for the South Atlantic based on the GTS 2020 timescale. (C) Schematic cross section showing correlation of the pre-salt stratigraphy between different isolated carbonate platforms penetrated by wells 1 and 3. Fm.—Formation.

Santos, Campos, and Espírito Santo basins offshore Brazil. Alternatively, these evaporites have been proposed to be as old as 120–125 Ma and associated with the Aptian Ocean Anoxic Event (OAE) 1a (Tedeschi et al., 2017). In addition to the challenges associated with absolute age calibration, extraction of important environmental conditions is hampered by the fact that the differentiation of the Barra Velha Fm and underlying Itapema Fm is largely based on lithostratigraphic correlation and log responses. However, given the time transgressive nature of deposition from the proximal to distal regions of the evolving Santos Basin during this period, there is potential for significant lithostratigraphic variability that limits the robustness of this approach alone.

The aim of this study is to investigate the potential for $^{87}Sr/^{86}Sr$ isotopes to provide a robust relative age framework for the Early Cretaceous lacustrine carbonates of the South Atlantic, and to calibrate this with absolute age constraints of the uppermost sequence. Additional information provided through the integration of carbonate clumped isotope geochemistry allows us to identify samples that have been optimally preserved for age dating, and develop the first comprehensive picture of both the timing and paleo-environmental conditions associated with this remarkable epi-continental carbonate factory. While recent studies have attempted to investigate environmental conditions from analysis of these carbonates, they have all relied on characterization from one well and extrapolated to the entire pre-salt system. Furthermore, none of these studies have been able to move beyond a relative age framework for the stratigraphy on both the Brazilian and the conjugate West African margin with any degree of confidence. Here, we provide characterization of strata from

four wells, each from separate isolated carbonate platforms located 15–80 km apart that together span an area of ~6400 km^2 in the Santos Basin (Fig. 1). We focus our characterization predominantly on the upper section of the pre-salt stratigraphy because of the 15 million year uncertainty on the timing of the regionally important salt deposition. Any age constraint would also provide the first robust upper bracket for the pre-salt stratigraphy which subsequent studies can further refine through additional constraints on key geologic boundaries deeper within the stratigraphic column.

GEOLOGIC SETTING

Situated offshore central Brazil, the Santos Basin covers an area of ~350,000 km^2 (Ariza Ferreira et al., 2019), and developed as a result of the extension and breakup of Gondwanaland in the Early Cretaceous ca. 135–140 Ma (Karner et al., 2021; Rangel et al., 1994). Like all the South Atlantic salt basins, the pre-salt of the Santos Basin is dominantly lacustrine in origin, with the Florianopolis High thought to provide a palaeogeographic barrier against marine intrusions from the South Atlantic Ocean. The initial sediments filling the basin are volcanics and volcaniclastics of the approximately Hauterivian aged Camboriú Fm underlying alluvial fans and lacustrine shales of the Piçarras Fm that is thought to be Barremian in age (Moreira et al., 2007). This was followed by the Itapema Fm, which comprises lacustrine shales and coquina-dominated carbonate reservoirs that represent the first significant deposition of carbonate in the pre-salt stratigraphy. The penultimate phase of deposition comprises shales and carbonates of the Barra Velha Fm. Finally, marine ingress drove the deposition of evaporites of the Ariri Fm (Moreira et al., 2007; Rodriguez et al., 2018). Basin to sub-basin scale volcanic events punctuate the entire pre-salt record. Despite this, there is a paucity of detail in the literature on the nature and age of these events. As a result, there is considerable uncertainty surrounding the absolute timing of Itapema through Ariri deposition, which could range from Barremian to Aptian-Albian in age (Moreira et al., 2007; Szatmari et al., 2021).

While absolute age correlation is challenged given the non-marine setting and the lack of direct age constraints on the carbonate intervals within the upper section of the stratigraphy, biostratigraphic constraints have been shown to be able to subdivide the lacustrine record on both sides of the Atlantic (Bate, 1999). The Itapema Fm, for example, is characterized by the ostracod genera *Hourcquia* and some species of *Petrobrasia*, while the Barra Velha Fm is characterized by a lower diversity of ostracods and dominated by species from the genera *Kroemmelbeincpris* and *Pattersoncpris* (Poropat and Colin, 2012a, 2012b). However, discrepancies within the ostracod zones between the Brazilian and the West African basins, coupled with the absence of absolute age calibration, creates challenges in using biostratigraphy to extrapolate globally beyond the Brazilian salt basins.

METHODS

Four wells made available by the Brazilian National Agency of Petroleum, Natural Gas and Biofuels were sampled, each from a different carbonate platform in the Santos Basin (Fig. 1). The wells were drilled in water depths of ~2000 m, and encountered the pre-salt carbonates at depths in excess of 5000 m total measured depth (3000 m subsea, see Table 1). Twenty samples were collected per well across the Barra Velha Fm and the Itapema Fm, where present, yielding a total of eighty samples for this study. Rock samples were obtained from conventional core plugs or from sidewall cores. Samples were selected for isotopic analysis following petrographic characterization to identify well preserved depositional fabrics and qualitatively assess the extent to which samples have experienced any diagenetic overprint. Thin sections of each sample were characterized using optical and scanning electron (JOEL 7600 with an Oxford Aztec energy dispersive spectroscopy (EDS) system) microscopy at ExxonMobil Upstream Integrated Solutions Company. Further, point counts were performed following the Gazzi-Dickinson method (Dickinson, 1985; Zuffa, 1980) to quantify the detrital and diagenetic mineralogy in ten samples (n = 300 points per thin section). These analysis captured the different lithologies and resulted in a paragenesis defined for each sample that comprised depositional and diagenetic fabrics based on observed superposition and cross-cutting relations between the various diagenetic phases. $^{87}Sr/^{86}Sr$ analysis was performed at Rutgers University (New Jersey, USA) for most samples, with a subset analyzed by Stony Brook University (New York, USA) to complete the data set. U-Pb age dating was performed at Stony Brook University applying the procedures described in Parrish et al. (2019). Carbonate clumped isotope analysis was performed by Isotomics Ltd, yielding $\delta^{13}C$, $\delta^{18}O$, and Δ_{47} for each sample.

Strontium Isotope Analysis

Sample preparation and procedures follow that described by Gamboa et al. (2019). Isotopes were run on a ThermoScientific Neptune Plus multicollector–inductively coupled plasma–mass spectrometer (MC-ICP-MS) at Rutgers University. Measurement of NBS 987 was included with all analyses and averaged 0.710245 ± 0.000006 (2σ, n = 40) by thermal ionization mass spectrometry (TIMS) or 0.710270 ± 0.000004 (2σ, n = 13) by MC-ICP-MS. Analyses by MC-ICP-MS were then corrected based on those values of NBS 987 values to match those of the TIMS instrument. The Sr was separated from the matrix in the rock samples by ion chromatography using 80 uL of Sr-spec resin (Eichrom) using 2 M nitric acid to remove major elements, 7 M to remove Ba in the rock samples, and recover Sr in the water. A subset of $^{87}Sr/^{86}Sr$ analyses were run on the samples used for U-Pb dating at Stony Brook University. Sr was separated using Sr-spec resin, washing with 2 M nitric acid and eluting with water. No correction was made since the TIMS analyses for NBS 987 averaged 0.710248 ± 0.000011 (2σ external, n = 12) which is identical to the recommended value (McArthur et al., 2001).

U-Pb Analysis

Core samples were slabbed and polished for laser ablation–inductively coupled plasma–mass spectrometry (LA-ICP-MS). A New Wave 213 laser system was coupled to an Agilent 7500cx for the LA-ICP-MS analyses using settings that are shown in Supplemental Table S1[1]. The NIST 612 soda glass standard was used for element analyses as well as for Pb isotope fractionation correction. The WC-1 calcite reference material (Roberts et al., 2017) was used for the U/Pb fractionation correction. Small element maps were made across fabrics to examine U/Pb in the context of mineralogy using major elements (Ca, Mg, and Si). Based on the element maps, areas with favorable U/Pb ratios were analyzed by spot LA-ICP-MS analyses using a 120 μm spot size. Spots on NIST 612, WC-1, and an internal secondary standard, Barstow, were analyzed at the beginning, between every 10 spots, and at the end of the analytical sessions. U-Pb isotope dilution (ID) analyses using a ^{205}Pb-^{236}U spike was performed on a set of four samples with favorable LA-ICP-MS U-Pb results. LA-ICP-MS data were reduced in Iolite (Paton et al., 2011) and ID data were reduced in PbDat (Ludwig, 1993). All of the U-Pb data (LA-ICP-MS and ID) were plotted on Tera Wasserberg isochrons using IsoExcel (Ludwig, 2003) or IsoplotR (Vermeesch,

[1]Supplemental Material. Methods, models, and all data and supporting figures. Please visit https://doi.org/10.1130/GSAB.S.19699822 to access the supplemental material, and contact editing@geosociety.org with any questions.

TABLE 1. Sr CONCENTRATION AND $^{87}Sr/^{86}Sr$ DATA ALONGSIDE THE STABLE CARBON AND OXYGEN ISOTOPE DATA ACQUIRED FOR THE PRE-SALT CARBONATES OF THE SANTOS BASIN, OFFSHORE BRAZIL

Field	Depth (m)	Depth from top BV (m)	Sr (ppm)	±1SE	$^{87}Sr/^{86}Sr$	±1SE	$\delta^{13}C$ (PDB)	±1SE	$\delta^{18}O$ (VPDB)	±1SE	Δ_{47}	±1SE	Temperature (°C)	Minus (°C)	Plus (°C)
1	5115.6	16.0	308.1	4.0	0.7135	0.00000	1.22	0.003	0.15	0.006	0.5731	0.0141	72	7	7
1	5117.2	17.6	1227.7	19.0	0.7135	0.00000	3.52	0.003	0.30	0.008	0.6596	0.0210	36	7	8
1	5120.5	20.9	2836.9	36.2	0.7136	0.00000	nd	nd	nd	nd	nd	nd	nd	nd	nd
1	5121.1	21.5	2359.6	21.2	0.7135	0.00000	3.07	0.003	–0.40	0.008	0.5588	0.0194	79	10	10
1	5130.6	31.0	1870.2	24.4	0.7139	0.00001	2.84	0.004	2.97	0.006	0.6065	0.0135	57	6	6
1	5136.9	37.3	1984.9	24.1	0.7141	0.00000	4.04	0.004	0.35	0.006	0.5976	0.0129	60	6	6
1	5140.4	40.8	2402.2	32.6	0.7135	0.00000	nd	nd	nd	nd	nd	nd	nd	nd	nd
1	5192.6	93.0	2819.0	42.7	0.7134	0.00000	3.31	0.002	2.44	0.005	0.6041	0.0219	58	9	10
1	5241	141.4	1609.2	17.0	0.7137	0.00000	3.26	0.015	1.70	0.004	0.6138	0.0166	53	7	7
1	5289	189.4	2000.2	28.6	0.7135	0.00001	2.55	0.003	1.66	0.012	0.5707	0.0204	73	10	10
1	5385	285.4	2690.9	22.0	0.7132	0.00000	nd	nd	nd	nd	nd	nd	nd	nd	nd
2	5325.5	9.6	3652.4	27.1	0.7133	0.00000	nd	nd	nd	nd	nd	nd	nd	nd	nd
2	5338	22.1	1520.9	17.2	0.7132	0.00000	1.02	0.004	–0.62	0.007	0.5749	0.0140	71	7	7
2	5345.5	29.6	3330.1	32.3	0.7136	0.00000	2.81	0.002	0.42	0.005	0.5720	0.0125	72	6	6
2	5363	47.1	2475.6	30.7	0.7133	0.00000	0.62	0.004	–0.84	0.007	0.5733	0.0182	72	9	9
2	5370.5	54.6	2690.0	27.9	0.7136	0.00001	2.23	0.006	–0.82	0.009	0.5984	0.0143	60	6	6
2	5373	57.1	2701.2	46.9	0.7132	0.00001	1.53	0.002	2.41	0.005	0.5843	0.0161	66	7	8
2	5383	67.1	2390.6	29.3	0.7131	0.00000	2.08	0.003	0.52	0.005	0.5933	0.0140	62	6	6
2	5480.5	164.6	2483.2	39.8	0.7133	0.00000	0.66	0.005	–2.39	0.006	0.5492	0.0125	84	7	7
2	5495.5	179.6	2505.9	27.5	0.7136	0.00000	–0.29	0.007	–2.87	0.007	0.5786	0.0125	69	6	6
2	5495.5	179.6	2505.9	27.5	0.7136	0.00000	–0.27	0.003	–2.59	0.003	0.5817	0.0128	68	6	6
2	5591	275.1	1583.6	9.2	0.7115	0.00001	nd	nd	nd	nd	nd	nd	nd	nd	nd
2	5722	406.1	794.9	7.3	0.7112	0.00000	nd	nd	nd	nd	nd	nd	nd	nd	nd
2	5740	424.1	508.9	5.3	0.7118	0.00000	–1.13	0.005	–6.27	0.009	0.5867	0.0202	65	9	10
2	5740	424.1	508.9	5.3	0.7118	0.00000	–1.07	0.002	–6.15	0.004	0.5944	0.0136	62	6	6
2	5745	429.1	1063.2	12.5	0.7111	0.00000	1.16	0.003	0.50	0.005	0.5909	0.0143	63	6	7
2	5753	437.1	1984.1	17.4	0.7113	0.00000	1.15	0.011	–0.44	0.005	0.5744	0.0151	71	7	8
3	5406	13.6	1170.6	9.6	0.7132	0.00001	1.70	0.013	–0.14	0.004	0.5753	0.0136	71	6	7
3	5420	27.6	nd	nd	0.7134	0.00001	1.84	0.002	1.08	0.005	0.6348	0.0123	45	5	5
3	5500	107.6	1589.2	19.9	0.7128	0.00000	1.49	0.004	3.59	0.008	0.6014	0.0145	59	6	6
3	5549.3	156.9	2607.5	16.8	0.7129	0.00000	2.23	0.004	0.76	0.007	0.6152	0.0191	53	8	8
3	5550.4	158.0	1047.6	12.4	0.7130	0.00000	1.21	0.003	–3.07	0.006	0.6532	0.0131	38	5	5
3	5562.8	170.4	156.9	1.0	0.7121	0.00000	–1.62	0.004	0.91	0.009	0.6311	0.0112	47	4	4
3	5563.5	171.1	45.2	0.7	0.7125	0.00001	nd	nd	nd	nd	nd	nd	nd	nd	nd
3	5564.3	171.9	1510.7	16.2	0.7125	0.00000	nd	nd	nd	nd	nd	nd	nd	nd	nd
3	5565.4	173.0	1662.3	18.8	0.7119	0.00000	nd	nd	nd	nd	nd	nd	nd	nd	nd
3	5581	188.6	1244.6	9.1	0.7122	0.00000	2.38	0.003	1.82	0.006	0.5306	0.0138	94	8	8
3	5581	188.6	1244.6	9.1	0.7122	0.00000	2.70	0.002	2.46	0.004	0.5366	0.0141	91	8	8
3	5619	226.6	984.5	9.5	0.7121	0.00000	1.42	0.004	–0.49	0.006	0.5955	0.0137	61	6	6
3	5708	315.6	967.5	11.2	0.7121	0.00000	nd	nd	nd	nd	nd	nd	nd	nd	nd
3	5729.5	337.1	2067.5	15.1	0.7118	0.00001	1.76	0.003	0.70	0.004	0.5620	0.0133	77	7	7
4	5336.5	4.9	678.0	5.0	0.7128	0.00000	1.51	0.002	0.19	0.005	0.5762	0.0150	70	7	7
4	5367.7	36.1	1021.1	10.4	0.7124	0.00000	1.98	0.003	0.42	0.005	0.6119	0.0103	54	4	4
4	5370.5	38.9	1256.2	17.0	0.7113	0.00000	nd	nd	nd	nd	nd	nd	nd	nd	nd
4	5381.7	50.1	1875.2	20.6	0.7126	0.00000	1.78	0.004	0.94	0.008	0.6002	0.0147	59	6	7
4	5387.6	56.0	2300.0	21.5	0.7118	0.00001	nd	nd	nd	nd	nd	nd	nd	nd	nd
4	5444.4	112.8	1878.4	20.8	0.7122	0.00001	nd	nd	nd	nd	nd	nd	nd	nd	nd
4	5476.9	145.3	1869.9	20.8	0.7122	0.00001	1.17	0.003	–0.43	0.006	0.5644	0.0126	76	6	7
4	5509.6	178.0	2767.4	29.1	0.7120	0.00000	1.86	0.001	0.23	0.005	0.6008	0.0182	59	8	8
4	5514.6	183.0	2690.1	34.4	0.7121	0.00001	1.36	0.004	–0.20	0.008	0.5725	0.0134	72	6	7
4	5516.7	185.1	911.3	11.4	0.7114	0.00000	2.33	0.004	1.82	0.008	0.5927	0.0143	63	6	7
4	5546.3	214.7	2322.1	21.8	0.7111	0.00000	nd	nd	nd	nd	nd	nd	nd	nd	nd
4	5570.9	239.3	1217.3	11.2	0.7113	0.00000	2.67	0.001	1.48	0.006	0.6327	0.0130	46	5	5

Notes: BV—Barra Velha Fm.; SE—standard error; PDB—Pee Dee belemnite; VPDB—Vienna Pee Dee belemnite; nd—no data.

2018). All ages included and discussed in this study are isochron ages reported at the two standard deviation confidence level.

Carbon and Oxygen ($\delta^{13}C$ and $\delta^{18}O$) Isotope Analyses

Forty powdered carbonate samples spanning the Barra Velha Fm and, where present, the Itapema Fm were analyzed at the California Institute of Technology in spring 2019. Samples were examined by binocular microscope to make an initial estimate of the proportions of carbonate and contaminant phases. Isotopic analyses ($\delta^{13}C$, $\delta^{18}O$, and Δ_{47}) were then performed on a custom-made automatic vacuum line attached directly to a Thermo MAT 253 mass spectrometer (Passey et al., 2010). All analyses were performed by phosphoric acid digestion using an automated common acid bath held at 90 °C. Samples were loaded into silver capsules, which were placed into an automated multi-sample chamber; a stepper motor dropped them individually into the heated acid. Evolved CO_2 was passed through a glass trap held in a dry-ice/ethanol slush to remove co-evolved H_2O and other condensable contaminants, and collected in a glass trap immersed in liquid nitrogen, after which CO_2 was entrained in helium and passed through a chilled, packed column of Porapak resin, held at 253 K. Concurrent extractions using the same equipment and methods on two intra-laboratory calcite standards ("CIT Carrera" and "TV04") were used to test consistency of the data set with long-term averages for these standards.

Each aliquot of CO_2 was analyzed on a Thermo Fisher 253 isotope ratio mass spectrometer for the ratios, $(^{13}C^{16}O_2 + {}^{12}C^{17}O^{16}O)/{}^{12}C^{16}O_2$, $(^{12}C^{18}O^{16}O + {}^{13}C^{17}O^{16}O + {}^{12}C^{17}O_2)/{}^{12}C^{16}O_2$, $(^{13}C^{18}O^{16}O + {}^{12}C^{18}O^{17}O + {}^{13}C^{17}O_2)/{}^{12}C^{16}O_2$ and $(^{12}C^{18}O_2 + {}^{13}C^{18}O^{17}O)/{}^{12}C^{16}O_2$, and were subjected to standard ion correction schemes to $\delta^{13}C_{\text{Vienna Pee Dee belemnite (VPDB)}}$, $\delta^{18}O_{\text{Vienna standard mean ocean water (VSMOW)}}$ of CO_2 and the Δ_{47} value of CO_2 (here reported relative to the "absolute reference frame"; Dennis et al., 2011). Samples were evaluated for their Δ_{48} values to assess the purity of extracted, cleaned gases. All values are reported with ±1 standard error, based on the reproducibility of several periods of mass spectrometric integration that contributed to the reported values; Δ_{47} errors also include propagated errors in the reference frame of heated and equilibrated gases.

We calculated the $\delta^{18}O_{VPDB}$ value of reactant based on the measured value of evolved CO_2 using an acid digestion fractionation factor

appropriate for calcite at our reaction temperature of 90 °C. We report apparent temperatures corresponding to the corrected Δ_{47} values using the experimental temperature calibration of Bonifacie et al. (2017). We analyzed 26 carbonate reference standards over the course of this study; results of these measurements agree with long-term accepted average values, and therefore, no corrections were made to this data set to account for systematic methodological errors. Similarly, 27 gases equilibrated at known temperatures were analyzed to establish the absolute reference frame used for correction for mass spectrometric artifacts. Standard reproducibility of a Carrara marble was 2.091‰ ± 0.061‰, −2.002‰ ± 0.091‰, and 0.399‰ ± 0.011‰ for measured $\delta^{18}O$, $\delta^{13}C$, and Δ values, respectively, based on one standard deviation error, as compared to the long-term Δ_{47} average for this standard of 0.352‰ (in the Ghosh et al., 2006 or "Caltech" intralaboratory reference frame). Errors in apparent temperature for each sample are asymmetrically distributed about the reported value because apparent temperature is a nonlinear function of clumped isotope composition.

RESULTS

Petrographic Observations

The carbonate samples obtained for this study are heterogeneous, with a great diversity of lithologies observed in the four carbonate platforms. The primary fabrics include shrub boundstones (or boundstone dominated fabric, see Figs. 2A and 2B), spherulite-bearing mudstones (mud-dominated facies, Figs. 2C and 2D), and grainstone dominated fabrics (Figs. 2E and 2F) with a significant range of diagenetic overprint (none to completely overprinted, see Fig. 3). Abundant Mg-rich clays occur in both the shrub boundstone and mudstone lithologies and are typically limited within the grainstone dominated lithologies.

Primary fabrics: Shrub boundstone lithologies (Figs. 2A and 2B) typically display calcic shrubs that are sectored and can bear small circular voids (100–500 μm) and occasional sinuous to straight, parallel-sided channels. The shrubs have a fascicular optical habit and are occasionally recrystallized to bladed and or equant sparry calcite (500–1000 μm) (Fig. 2B). A vertically stacked, repeated sequence occurs within some thin sections of shrub boundstone laminations of calcite dominated precipitation, dolomite dominated precipitation, and finally Mg-smectite dominated precipitation.

The mudstone-dominated fabrics typically contain spherulites that occur as spherical forms (Fig. 2C) and can have a radial-fibrous optical habit in clay-rich lamination where diagenetic overprints are limited (Fig. 2D). Spherulites typically have a more elongated, asymmetrical form in lamina with lower clay volumes. These asymmetrical forms are similar in shape to shrubs and can be difficult to distinguish in samples that have been significantly diagenetically altered (e.g., Fig. 2E). The clay groundmass in the spherulitic mudstones commonly has fabrics consistent with post-depositional physical compaction (e.g., stylolites). If the spherulite fraction is great enough, the spherulitic mudstones become spherulite-supported packstones.

The grainstone-dominated fabrics are largely formed from shrub and spherulite allochems (Figs. 2E and 2F), but occasionally contain chert fragments, mud intraclasts and/or rare volcanic lithic fragments. The grainstone lithologies provide evidence for current transport and sedimentation of allochems derived from shrub boundstone and spherulitic mudstone environments of deposition. Transport appears to effectively winnow the clay-size fraction from the mobilized sediments.

Porosity: Average helium porosity in the studied samples range from 9.4% to 15% depending on lithology: shrub boundstones 15 ± 3.3%, mudstone dominated 9.4 ± 4.0%, and grainstone dominated 14 ± 4.4% (mean ± 2σ). Shrub boundstones and grainstones typically have macro-porosity occurring between grains or shrubs that can be enhanced by secondary dissolution. Mudstones and clay-rich shrub boundstones have significant micro-porosity. The presence of corroded inter-shrub clay particles and jagged margins along the calcite shrubs suggest that dissolution of mud and calcite has generated secondary porosity.

Diagenesis: The first diagenetic process we observe is the dissolution of primary fabrics, in particular Mg-smectite and to a lesser degree dissolution of the carbonate components. Significant vuggy and moldic porosity is present in samples where this has occurred (Fig. 3A). The first diagenetic products we observe are one of or a combination of dolomite, calcite or, in some cases, silica cements filling secondary porosity. Dolomite is microcrystalline to rhombic and fills secondary porosity that develops as a result of dissolution of Mg-clay (Figs. 3B–3D). The earliest form of diagenetic calcite we observe is a continuous isopachous calcite cement that coats individual grains in some grainstones, and in rare cases, may cement multiple grains together to form small grapestone clasts. In many boundstone and mudstone dominated fabrics, we observe recrystallization of shrub boundstones and spherulites (Figs. 3A–3C). Finally, silica cement is also observed to immediately follow or be concomitant with dissolution of Mg-clays or carbonates in some samples. The earliest phase of silica cementation is in the form of microcrystalline silica (i.e., chert), which precipitates in secondary porosity in the same way as the microcrystalline dolomite and isopachous calcite cements above. This is followed by fibrous chalcedony that can be repetitively zoned, and is observed to rim secondary porosity that has not been replaced by the initial dolomite, calcite, or silica cements. In some cases, silicification has completely destroyed the primary fabric (e.g., Figs. 3E and 3F). While it is difficult to definitively reconcile the relative timing of these specific dolomite, calcite, and silica cements, they clearly occur prior to other crystal habits of the same minerals and as such represent the earliest forms of preserved diagenetic products.

In some samples, we observe later diagenetic phases of dolomite, calcite, and silica, and additional distinctive minerals. The latest diagenetic dolomite is in the form of a pore filling and fracture lining saddle dolomite. This form of dolomite displays a characteristic larger crystal size and curved crystal habit that allows it to be differentiated from the microcrystalline and rhombic dolomite described above. Similarly, we observe a transition to equant sparry calcite replacing earlier forms of calcite. This calcite is translucent in plain light and at times occurs after dolomitization. Finally, in some samples we observe a transition to mega quartz with a larger crystal size compared to the earlier microcrystalline and fibrous chalcedony (Fig. 3F). In core, mega quartz is often found within vugs that are lined with chalcedony and terminate in open pore space, and in thin section it is observed to fill remaining pore space (i.e., Figs. 2B and 3F). In addition to the transition in the character of these diagenetic products, these later phases are occasionally associated with metal sulfides (i.e., pyrite/maracasite and sphalerite), fluorite, an aluminum-phosphate-sulfate (APS) mineral that we found to be compositionally consistent with goyazite, barite/celestite, and dawsonite (Figs. 3G–3I, composition confirmed by EDS).

$\delta^{13}C$, $\delta^{18}O$, Δ_{47}, and $^{87}Sr/^{86}Sr$ Geochemistry

The $\delta^{13}C$ and $\delta^{18}O$ (VPDB) values of the carbonate samples display significant variability. In general, we observe a range in $\delta^{13}C$ from −1.6 to +4‰$_{VPDB}$ and a range in $\delta^{18}O$ from −6.3 to +3.6‰$_{VPDB}$ (n = 39). The Δ_{47} values for the entire data set range from 0.537 to 0.660‰, with a mean of 0.592‰. These values correspond to a range in apparent temperature from 36–91 °C, with a mean apparent temperature of 63 °C. The apparent temperatures display no systematic correlation with $\delta^{13}C$ and $\delta^{18}O$ (see Supplemental Figs. S32 and S33; see footnote 1). The $^{87}Sr/^{86}Sr$

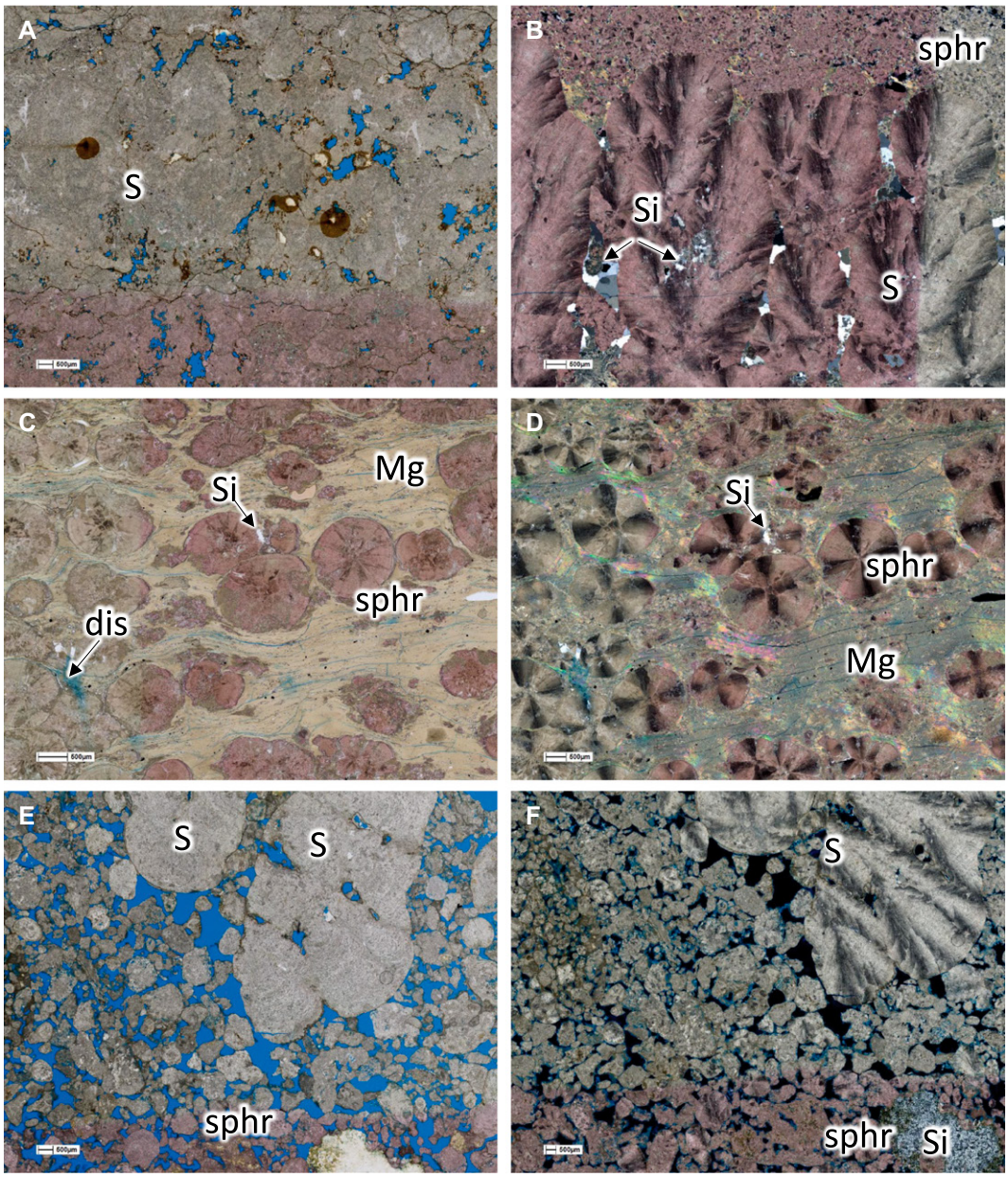

Figure 2. Dominant primary fabrics of pre-salt carbonate analyzed in this study from Santos basin, offshore Brazil: boundstone dominated fabric (A and B), spherulite-bearing mudstone (C and D), and grainstone dominated fabric (E and F). (A) Weakly stylolitized, very coarse shrub boundstone with primary fasicular optical habit and moderate vuggy porosity in plain light. (B) Very coarse shrub boundstone and medium spherulite-bearing mudstone with pore filling mega quartz (cross polar). (C) Spherulite-bearing mudstone in plain light and cross polar (D) showing the spherical form and radial fibrous nature of the spherulites. (E) Coarse to gravelly, shrub and spherulite grainstone with extensive interparticle porosity in plain light and (F) cross polar. (Mg—Mg-smectite; Dol—dolomite; S—calcite shrub; sphr—calcite spherulite; Si—as chert, chalcedony, and/or mega-quartz). All thin sections are stained with alizarin red so calcite is presented as pink in the images.

values of samples from all four wells in this study range from 0.7111 to 0.7141. All isotopic data is presented in Table 1.

U-Pb Dating

A subset of 19 samples, selected based on their stratigraphic positions and diagenetic histories, were analyzed by LA-ICP-MS to determine if they had favorable U/Pb ratios. Multiple maps were made across samples with complex fabrics to obtain information on all phases represented by the sample. Based on this initial screening, 15 samples were selected for more comprehensive LA-ICP-MS spot analyses in an effort to define isochron ages for the samples. This comprised of 11 samples from the Barra Velha Fm and four samples from the Itapema Fm based on the chronostratigraphic framework defined by $^{87}Sr/^{86}Sr$, facies and log correlations described above. Of the samples analyzed, a total of nine samples from the Barra Velha Fm and two samples from the Itapema Fm yielded ages (see Supplemental Material for more details). This analysis produced seven isochron ages, all from samples from the Barra Velha Fm, with a range from 114 ± 4.72 to 58.85 ± 10.74 Ma (Supplemental Table S3). Based on the spread of U/Pb and the mean square weighted deviation of the data, only three of these samples were selected for parallel additional analyses via isotope dilution thermal ionization mass spectrometry (ID TIMS).

Most of the samples analyzed by LA-ICP-MS are easily interpreted as non-depositional. However, a sample from well 1, taken from a depth of 37.3 m below the Ariri Fm, gives an isochron age from LA-ICP-MS of 114.46 ± 4.72 Ma. Similarly, a sample from well 3 taken from a depth of 27.6 m from the base of the Ariri Fm gives a LA age of 109.73 ± 9.26 Ma. Of the samples selected for ID TIMS, only one sample yielded a robust isochron age. This was a sample taken from well 3 at 27.6 m below the base of the Ariri Fm, and yielded an isotope dilution (ID) isochron age of 115.83 ± 1.56 Ma (Fig. 4). This is in good agreement with the isochron age obtained via LA-ICP-MS from the same sample of 109.73 ± 9.26 Ma described above.

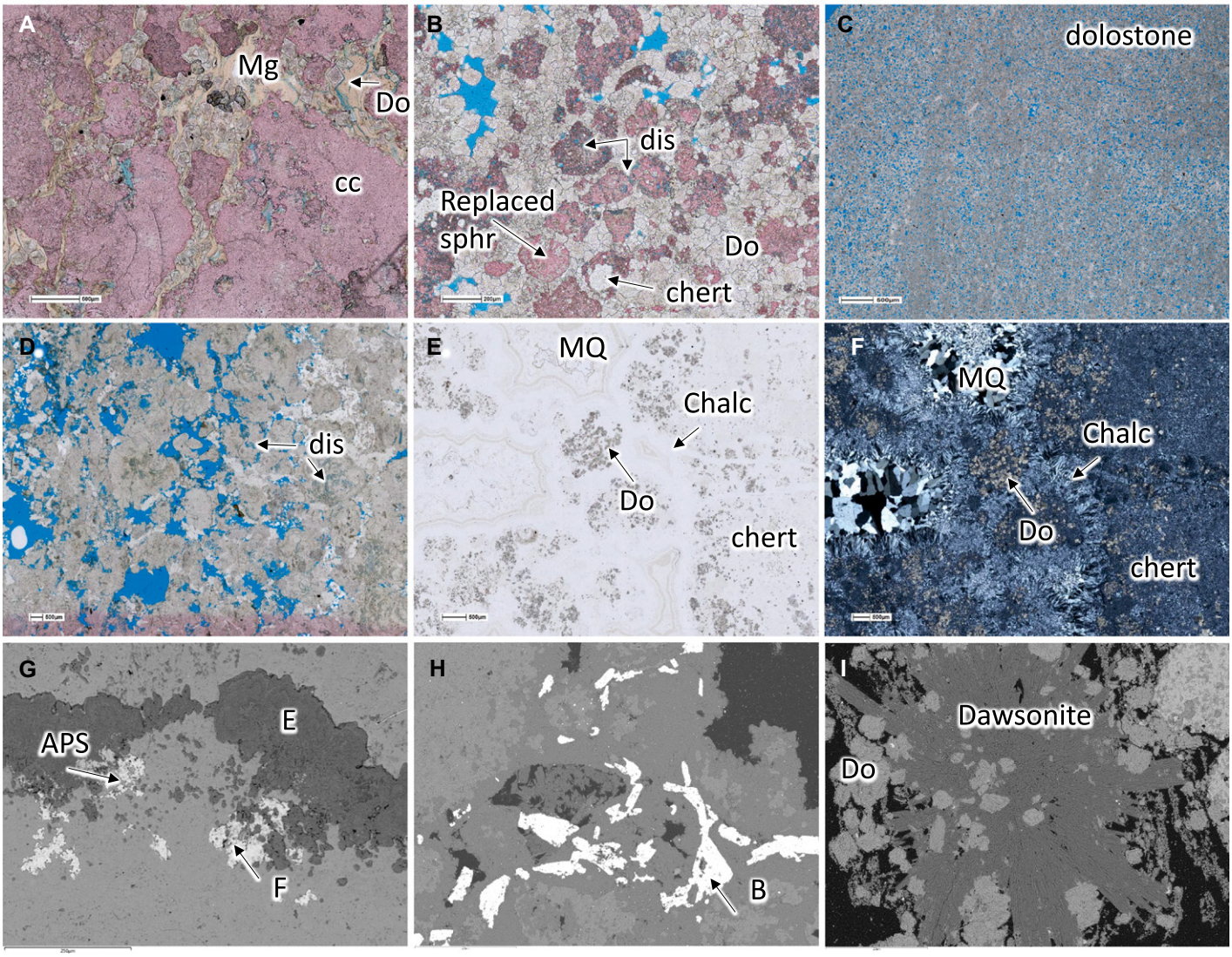

Figure 3. Range in diagenetic alteration of pre-salt carbonates from Santos basin, offshore Brazil. (A) Rhombic dolomite within Mg-smectite and recrystallized calcite shrubs. (B) Dolomitized shrub boundstone with evidence of replaced spherulites and dolomitization. (C) Extensively dolomitized fine to medium crystalline dolomite with vuggy to moldic to intercrystalline porosity. (D) Quartz and dolomitized shrub boundstone with extensive dissolution leading to vuggy porosity. (E) Completely silicified dolostone with limited to no visible porosity with all three forms of silica: chert, chalcedony (chalc), and mega quartz (MQ) in plain light and (F) cross poles. (G) Scanning electron microscope (SEM) backscatter image of sample containing fluorite (F) and an aluminum-phosphate-sulfate (APS) mineral compositionally similar to goyazite (APS). Fluorite and APS are commonly found at the margins of pores and especially dissolution enhanced pores. (E) designates epoxy-filled pore space. (H) SEM backscatter image of barite. (I) SEM backscatter image of sample containing dawsonite and rhombic dolomite (Mg—Mg-smectite; Cc—calcite; Do—dolomite; sphr—spherulite; dis—dissolution; chalc—chalcedony; MQ—mega quartz; B—barite; APS—goyazite; F—fluorite).

DISCUSSION

Petrographic Assessment of Primary Depositional Fabrics and Insights on Diagenetic Overprints

The samples of the Barra Velha Fm studied here display great variability in their composition, with facies that include shrub boundstones, re-worked shrub (dendritic) grainstones, spherulitic packstones, and fine-grained carbonate mudstones. These observations are consistent with previous studies that focused on this interval (e.g., Gomes et al., 2020; Wright, 2022; Wright and Barnett, 2020, 2015). Furthermore, these facies are consistent with those described by Saller et al. (2016) for the time equivalent stratigraphy of the conjugate Kwanza Basin, offshore Angola.

The petrographic observations described above suggest that the samples studied here have experienced a broad range in both the extent and the timing of diagenetic overprint. There is a clear distinction in the samples from those that experience relatively minimal alteration of depositional fabrics to those that have experienced almost pervasive replacement of primary fabrics by late-stage diagenesis. Diagenesis begins with an initial stage of dissolution, which is followed by or is concomitant with the precipitation of early diagenetic products that are dominated by

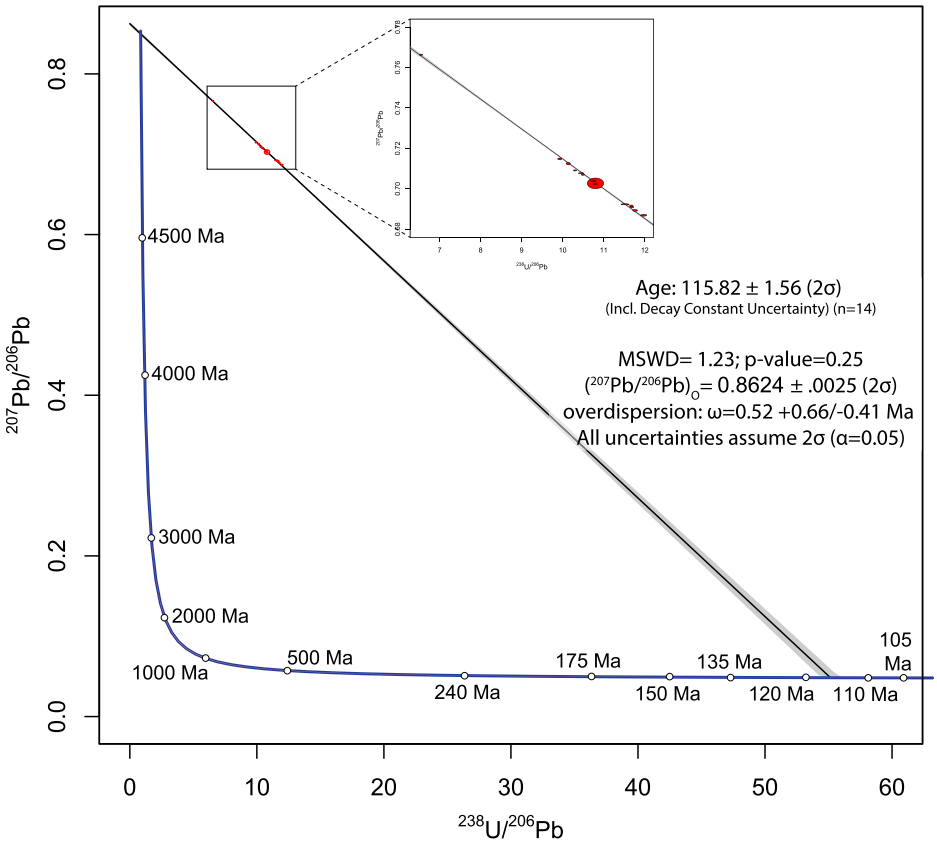

Figure 4. U-Pb isotope dilution (ID) isochron age obtained from a sample of the Barra Velha Formation in well 3 in the Santos Basin, offshore Brazil. MSWD—mean square weighted deviation; Incl.—including.

either dolomite, calcite, or silica cementation. This is followed by the precipitation of saddle dolomite, equant calcite, and/or mega quartz that in some cases occur approximately concurrent with minerals such as metal sulfides, dawsonite, and APS that are diagnostic of high temperature diagenesis or direct precipitation from hydrothermal fluids (e.g., Dill, 2001). While all samples were analyzed, samples that only display limited diagenetic overprint (e.g., primary depositional fabrics such as shrub boundstones and early silica or dolomite diagenetic phases) are considered favorable for age dating. In contrast, samples that included evidence of pervasive dolomitization, silicification, or APS minerals are interpreted to have been impacted by burial diagenesis or hydrothermal alteration and were considered less favorable to address the objectives of this study.

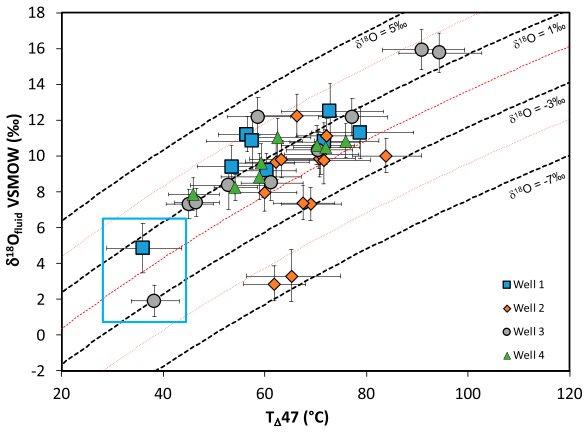

Figure 5. $\delta^{18}O_{fluid}$ against apparent clumped isotope temperature for the Barra Velha Fm and Itapema Fm carbonates analyzed in this study. The two coldest temperatures (<40 °C) in the blue box that we consider to reflect depositional conditions provide a range in lake water $\delta^{18}O_{fluid}$ of ~2–5‰$_{Vienna\ mean\ ocean\ water(VSMOW)}$. Clumped isotope temperatures above 40 °C are interpreted to reflect diagenetic alteration, and as such, the calculated $\delta^{18}O_{fluid}$ is not considered to be representative of true lake chemistry for those samples.

Constraints on the Conditions during the Terminal Stage of Lacustrine Carbonate Deposition

The lowest temperatures we report here of 36 ± 7 °C and 38 ± 5 °C measured from samples taken at depths of 17.6 m and 158 m from the top of the Barra Velha Fm in wells 1 and 3, both within the Barra Velha Fm, are consistent with the average clumped isotope temperature of carbonates reported for the time equivalent Codó Fm (Bahniuk et al., 2015). We suggest that these apparent temperatures record the original physico-chemical conditions of the giant pre-salt lake waters during deposition of these ancient lacustrine carbonates. From these apparent temperatures and independent measurement of $\delta^{18}O$ of the carbonates, we are able to calculate the $\delta^{18}O$ of the Santos Basin pre-salt lake water to be between +1.9 and +4.9‰$_{(VSMOW)}$ (Fig. 5) using the relationship of Kim and O'Neil (1997). These values are similar to the fluid $\delta^{18}O$ of +6‰$_{(VSMOW)}$ estimated for the time-equivalent conjugate pre-salt lakes from the Kwanza Basin of Angola (Saller et al., 2016). Such $\delta^{18}O$ fluid values are typical of modern lakes that have been subject to evaporation in a relatively hot, semi-arid to arid climate (Horton et al., 2016).

To quantify the extent of lake water evaporation needed to give rise to this range in $\delta^{18}O_{(VSMOW)}$ values, we developed a box model (see Supplemental Material for details) that calculates lake water $\delta^{18}O$ at a nearly constant lake level maintained by two river sources relative to constant evaporation. Our modeling suggests that such $\delta^{18}O$ values of lake water require a range in the extent of evaporation of 40%–56% at a semi-arid humidity of ~50%. Such evaporative conditions are consistent with an increasingly stressed environment that is also recognized by decreasing biodiversity in the lake fauna records (Antonietto et al., 2012; Bate, 1999). These authors concluded that the ostracod fauna identified in the Barra Velha Fm and time equivalent pre-salt stratigraphy in West Africa display a decrease in ornamented and robust shells. This impact on faunal morphology was also associated with a clear decrease in the diversity and abundance of the ostracod fauna in the period leading up to the deposition of the regional salt sequences. Our isotopic constraints of paleo lake chemistry are therefore consistent with observations in the ostracod record. Taken together, these results suggest that the pre-salt lakes became increasingly salinity stressed as a result of the prevailing climatic conditions during

deposition of the Barra Velha Fm (Antonietto et al., 2012; Bate, 1999).

While the clumped isotope temperatures and $\delta^{18}O$ isotope constraints on the paleo-depositional environment are the primary focus of this study, we recognize that the majority of the clumped isotope temperatures we measure are greater than 40 °C. Such values exceed estimates for reasonable earth surface conditions. Interestingly, these elevated temperatures are consistent with the only other reported clumped isotope temperatures of 46–73 °C discussed in Farias et al. (2019) for the Barra Velha Fm. We consider here four potential explanations for such elevated temperatures. One possibility, as proposed by Farias et al. (2019), is that these temperatures are indicative of the influence of hot springs discharged into the pre-salt lakes in the vicinity of carbonate precipitation based on samples that Farias et al. (2019) interpret to be primary textures free from the influence of diagenetic alteration. This concept essentially implies mixing between a hydrothermal fluid and lake water, with precipitation of carbonate occurring in the lake either in close proximity to or directly associated with hydrothermal fluid input. In such a scenario, one would expect to observe a mixing relationship between two end-members: a colder lake water characterized by lower clumped isotope temperatures and lower $\delta^{18}O$ values, and higher clumped isotope temperatures and a more isotopically enriched hydrothermal fluid. Such a relationship is observed in the study of Cruset et al. (2016) for mixing between low temperature meteoric fluids and higher temperature hydrothermal fluids during precipitation of fracture filling carbonates. However, as discussed above, we do not observe any co-variance between clumped isotope temperatures and $\delta^{18}O$ values in our samples.

A second possibility is that the apparent temperatures result from precipitation of these carbonates under non-equilibrium conditions due to rapid mineral growth or precipitation at high pH (e.g., Watkins and Hunt, 2015), as proposed by Pietzsch (2021). In such a scenario, the carbonates could be precipitating at surface conditions, but not recording such temperatures because of a kinetic control on the clumped isotope signatures during non-equilibrium precipitation. It is possible that changes in lake chemistry may give rise to conditions that are more or less favorable to equilibrium precipitation. Such effects are likely to become significant above pH 8.9 for tufa carbonates (Kele et al., 2015), which is consistent with the paleo-lake conditions that have been postulated to have supported the rapid precipitation of carbonate within the pre-salt lakes (e.g., Wright, 2022). However, any kinetic overprint would likely result in increasingly negative values of $\delta^{13}C$ and $\delta^{18}O$ if it represents a dominant process (Devriendt et al., 2017) and we do not observe such values in our data set. Furthermore, the range in $\delta^{13}C$ and $\delta^{18}O$ that we measure on these ancient pre-salt carbonates is similar to those found in a global compilation of modern lacustrine carbonates that are thought to precipitate under dominantly equilibrium conditions (Horton et al., 2016). This suggests that any kinetic isotope effect as a result of elevated pH in our data set is minor, if present at all.

A third possible explanation for the clumped isotope temperatures we report here above 40 °C is that they reflect the internal reordering of original depositional clumped isotope signatures through solid state diffusion as a result of exposure to high temperatures over geologic timescales (e.g., Lawson et al., 2018; Passey and Henkes, 2012; Shenton et al., 2015; Stolper and Eiler, 2015). The samples in this study were all obtained from depths in excess of 3000 m subsea. The subsurface ambient temperature, at the depths our samples were taken, ranged from 60–90 °C. However, our clumped isotope apparent temperatures display no trend with increasing depth in any of the studied wells (Table 1). Further, we observe a broad range in clumped isotope apparent temperatures despite the relatively narrow window of burial temperatures of 60–90 °C. As such, we suggest that there is no systematic alteration of the Δ_{47} studied samples as a result of exposure to elevated temperatures. Therefore, we consider the possibility that the elevated clumped isotope temperatures that we report here could be a result of burial diagenesis during either recrystallization of original carbonate phases or precipitation of new diagenetic products.

To test the hypothesis that diagenetic overprinting accounts for the range in clumped isotope temperatures we report here, we performed point counting of the mineralogies observed in a subset of ten samples. Samples were selected to represent the entire range of clumped isotope temperatures we observed from 36 ± 8 °C to 91 ± 8 °C. The results of the point counting can be found in Table 2. We chose to perform point counting instead of X-ray diffraction because this petrographic approach allows us to distinguish and quantify the relative amounts of the same mineral phase related with early depositional or later diagenetic events within the same sample (i.e., rhombic dolomite versus saddle dolomite). Using this method, we observed that the coldest clumped isotope temperatures are associated with samples that have the highest silica fraction (Fig. 6A). These samples dominantly contained microcrystalline silica, which is interpreted to form during the earliest stages of diagenesis. This correlation of what we interpret

TABLE 2. POINT COUNTING PETROGRAPHIC RESULTS FROM A SUBSET OF TEN SAMPLES FROM THE SANTOS BASIN, OFFSHORE BRAZIL WITH CLUMPED ISOTOPE TEMPERATURES RANGING FROM 36 ± 8 °C TO 91 ± 8 °C

		Grains				Cements							Replacements						Porosity				Total
Field	Depth (m)	Sphr	Shrubs	Carb fossil	Qtz grain	Detrital clay*	Cc	Fe-Cc	Dol	Mg-clay	Barite	Chert	Chalc	Mega Qtz	Daw	Py	Kao	Cc	Dol	Mg-clay	Chert	Mega Qtz	Inter-granular primary	Intra-granular secondary	Intra-granular primary	Inter-granular secondary	
1	5117	22.9	16.1						5.2	16.1		12.9		18.9			6.8		0.4	0.8							100
2	5346	30.4	24.8		2.0		2.8		18.8			1.2			1.2			0.8	4.4	1.2			6.8	1.6	3.6	0.4	100
2	5381	34.0	1.2						47.6	2.4				0.8					2.8				0.8	0.4	0.8	9.2	100
2	5496	43.6	0.8						36.0		0.4	0.8							8.0				3.6	0.4		6.4	100
2	5740	7.2	2.0	0.4	14.3	1.2	3.6	12.4	54.2	0.4	0.4	30.7	15.5	6.4		4.0			0.4								100
3	5550	9.2	16.7						7.6			0.4						2.0	2.8		5.6	1.6	1.6		0.4	1.6	100
3	5581												0.4	0.8					75.1				9.2		0.8	12.5	100
3	5619			37.6			42.4	0.4	0.8	0.4													8.8	0.4	0.4	7.6	100
4	5477	38.5			2.8				36.9	3.2									1.2		0.8		3.2	3.6		9.9	100
4	5571			48.6			18.0		3.3			3.7		14.3					5.3		0.8	1.6	0.4			4.1	100

Notes: Results are classified by either depositional grains, cements, replacements, or porosity (primary and diagenetic products). Sphr—spherulites; Carb—carbonate; Qtz—quartz; Cc—calcite; Dol—dolomite; Chalc—chalcedony; Daw—dawsonite; Py—pyrite; Kao—kaolinite.
*Includes micas.

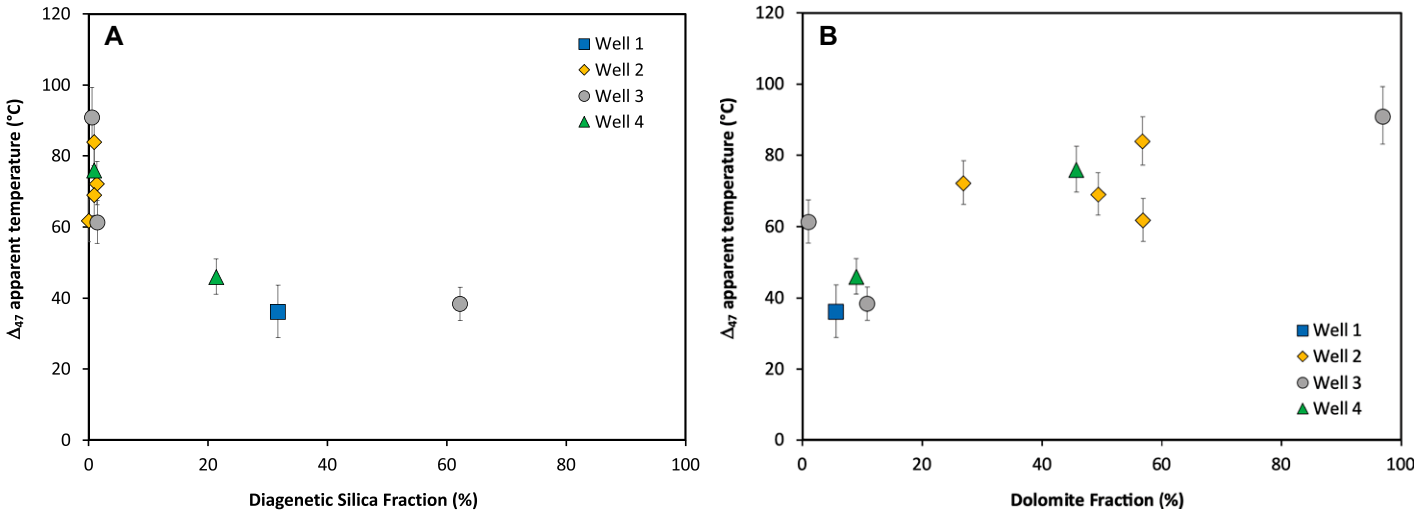

Figure 6. Apparent clumped isotope temperature against (A) diagenetic silica fraction, and (B) dolomite fraction determined via point counting for a subset of 10 samples from the Santos Basin analyzed in this study. Data is provided in Table 2. We observe a positive relationship between fraction of dolomite in the sample and the carbonate clumped isotope temperature. Similarly, samples with diagenetic silica fractions of greater than 20% appear to record colder clumped isotope temperatures based on the small sub-set of samples that were subjected to point counting.

to be minimally altered depositional clumped isotope temperatures of less than 40 °C with early silica diagenesis is consistent with the findings of De Boever et al. (2017), who studied alteration signatures of non-marine carbonates. We suggest that this early silica phase reduced available porosity of samples, reducing relative permeabilities and acting as a barrier for fluid related diagenesis during burial. Similarly, we observed that the hottest clumped isotope temperatures are associated with samples with the highest dolomite fraction (Fig. 6B). As discussed above, while dolomite precipitation appears to be a product of both early and later diagenesis, this data suggests that extensive dolomitization is associated with higher temperature diagenesis.

Given that we interpret the clumped isotope temperatures we measure in excess of 40 °C to be a product of burial diagenesis, it is important to note that the range in $\delta^{18}O$ fluid values that we calculate of +5 to +16‰$_{(VSMOW)}$ (Fig. 5) are not representative of the paleo lake chemistry that prevailed during deposition of the Barra Velha Fm. This interpretation also challenges the suggestion of Farias et al. (2019) that the range of fluid $\delta^{18}O$ that they calculate of +5‰ to +11‰$_{(VSMOW)}$ from clumped isotope temperatures of 46–73 °C are an accurate prediction of paleo lake chemistries and depositional temperatures. Given that the conversion of metastable carbonate mineral phases can occur without significant dissolution and re-precipitation, even samples that display no clear visual evidence of alteration may have been modified during diagenesis (De Boever et al., 2017). This perhaps highlights the challenges associated with identifying relatively pristine samples that capture true depositional conditions in large parts of the geologic record that have experienced significant burial.

Absolute Age Framework for the South Atlantic Salt Basins

$^{87}Sr/^{86}Sr$ geochemistry has been increasingly applied to lacustrine deposits that lack diagnostic age indicators to aid in chronostratigraphic correlation (Baddouh et al., 2017; Hart et al., 2004). The $^{87}Sr/^{86}Sr$ values we report of 0.7111–0.7141 are consistent with previous studies that investigated the $^{87}Sr/^{86}Sr$ for the Barra Velha (0.712–0.714) and Itapema (0.711–0.712) Fms of the Santos Basin (Pietzsch et al., 2018, 2020), as well as the time contemporaneous Macabu and Coqueiros Fms of the Campos Basin (Lima et al., 2020). The origin of the highly radiogenic $^{87}Sr/^{86}Sr$ values is not well understood, but it is a consistent feature of all the pre-salt carbonates studied to date. As such, it likely reflects an inherent compositional property of the pre-salt depositional environment, and not post-deposition alteration that is likely to be highly variable across the carbonate platforms studied so far. The observation of such radiogenic $^{87}Sr/^{86}Sr$ values also provides further support for a non-marine depositional environment for the pre-salt carbonates given that the $^{87}Sr/^{86}Sr$ values of Aptian seawater ranges from ~0.7074 to 0.7072 (Jones and Jenkyns, 2001).

Importantly, the decrease in $^{87}Sr/^{86}Sr$ from the Barra Velha Fm to the Itapema Fm is also associated with a change in facies from carbonate grainstones to coquina. This provides strong calibration of the Sr isotope stratigraphic correlations that can be applied to more mud dominated sections that do not capture the diagnostic carbonate facies-based transition. As such, the $^{87}Sr/^{86}Sr$ geochemistry of the carbonates provides the basis for a chemostratigraphic framework to differentiate the major sequences within the pre-salt, and in particular, distinguish the Barra Velha Fm from the Itapema Fm. In Figure 7, we present $^{87}Sr/^{86}Sr$ profiles alongside facies classification and petrophysical logs for each well. Depths are plotted relative to the base of the Ariri Fm to normalize for differences in the measured depths of these isolated carbonate platforms across the Santos Basin relative to a common stratigraphic marker. We observe greater variability in the $^{87}Sr/^{86}Sr$ values in wells 2, 3, and 4 (0.711–0.714) than in well 1 (0.7132–0.7141). In these wells, the $^{87}Sr/^{86}Sr$ profile exhibits a general decrease with increasing depth from values close to 0.714 immediately beneath the evaporites of the Ariri Fm to values closer to 0.711 in the deepest samples. This suggests that both the Barra Velha and Itapema Fms are represented in these wells, while only the Barra Velha Fm is present in well 1. We use the different $^{87}Sr/^{86}Sr$ values between the Bara Velha and Itapema Fms described above to estimate the transition depth of these formations for wells 2, 3, and 4, focusing on samples where there is a systematic shift to lower $^{87}Sr/^{86}Sr$ values across

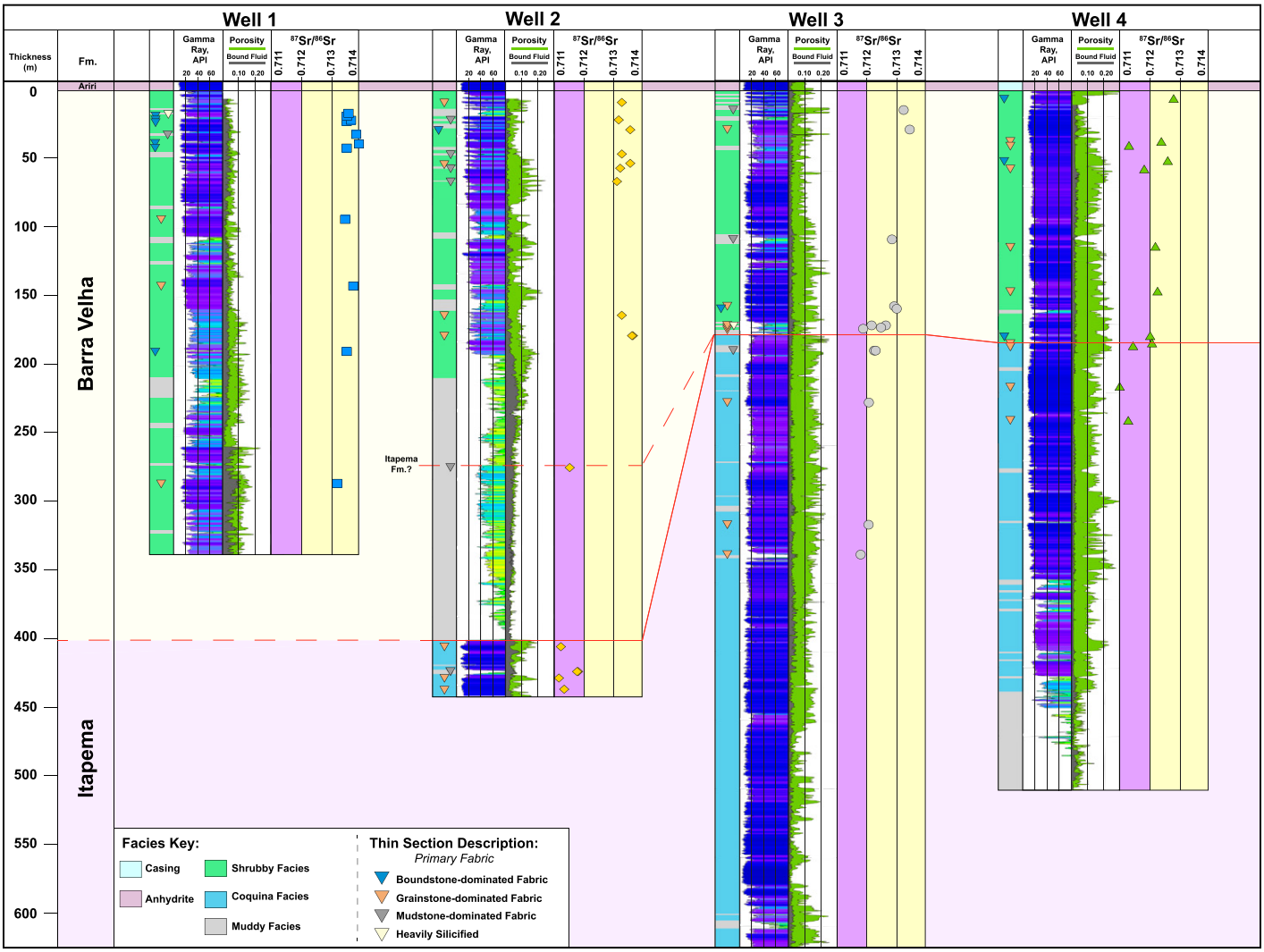

Figure 7. Relative age framework provides differentiation of the Barra Velha and Itapema formations of the Santos Basin, offshore Brazil. Fm.—Formation; API—American Petroleum Institute.

this boundary. Isolated shifts that occur within a given formation likely represent overprinting of the original depositional $^{87}Sr/^{86}Sr$ signature. One such process that has been demonstrated to result in a transition to lower values is hydrothermal alteration. Lima et al. (2020) showed that the $^{87}Sr/^{86}Sr$ composition of what they interpret to be hydrothermal saddle dolomite is lower (from 0.7111 to 0.7126) than the host rocks of the Macabu Fm.

In general, the $^{87}Sr/^{86}Sr$ isotope profiles we obtained display relatively consistent structure with depth across all four wells. We integrate observations from lithostratigraphy and logs to further refine this chemostratigraphic correlation and align on a depth for the Barra Velha-Itapema transition. For example, in well 2, there is a lack of resolution in the $^{87}Sr/^{86}Sr$ profile with a single measured $^{87}Sr/^{86}Sr$ value between 180 m and 406 m. In this case, we observe a shift in $^{87}Sr/^{86}Sr$ from 0.7136 to 0.7115 at a depth of 275 m that represents a candidate depth for the transition into the Itapema Fm. However, this is not consistent with the onset of coquina facies and a marked shift in the gamma ray that occurs at a depth of 400 m below the base of the Ariri Fm that we interpret to mark the true transition from the Barra Velha to Itapema Fms (Fig. 7). In wells 3 and 4, the transition between the Barra Velha and Itapema Fms is interpreted to occur at ~180 m below the Ariri Fm. This interpretation is supported by a consistent response of gamma ray, lithology transition from to coquina facies and a decrease in $^{87}Sr/^{86}Sr$ values at this depth.

We took advantage of the chemo and lithostratigraphic differentiation of the Barra Velha and Itapema Fms discussed above to select samples from roughly time equivalent stratigraphy from different carbonate platforms for U-Pb age dating (Fig. 7). Fifteen samples from the Barra Velha Fm were analyzed for U-Pb dating. We focus our discussion here on samples that yielded isochron ages within a realistic range for depositional ages of these pre-salt carbonates (a full discussion is provided in the Supplemental Material for all samples), and the uncertainty on the ages discussed is at the two-sigma (2σ) confidence interval. Two samples from the Barra Velha Fm from different carbonate buildups (wells 1 and 3) give overlapping ages of ca. 115 Ma. The sample from well 1, taken from a depth of 37.3 m below the Ariri Fm, gives an isochron age from LA-ICP-MS age of 114.46 ± 4.72 Ma. The sample from well 3, at a depth of 27.6 m from the base of the Ariri Fm, gives a LA age of 109.73 ± 9.26 Ma and an isotope dilution (ID) isochron age of

115.83 ± 1.56 Ma as described above. The sample successfully dated from well 1 comprises a very fine grained peletal and spherulite grainstone that has early dolomite cement present in secondary porosity. Similarly, the sample from well 3 represents a laminated, fine grained peletal grainstone that has also experienced early dolomitization. This petrographic assessment of alteration is further supported by the $^{87}Sr/^{86}Sr$ values of these samples of 0.7141 and 0.7134, respectively, which show no evidence of low $^{87}Sr/^{86}Sr$ values that are diagnostic of hydrothermal alteration. Finally, the clumped isotope apparent temperatures of these two samples were 60 ± 6 °C and 45 ± 5 °C, respectively. While the clumped isotope temperatures are not representative of depositional conditions, this combination of petrographic and isotopic analysis suggests that these rocks have experienced only minor levels of early burial diagenesis. As such, we are confident that the U-Pb ages that we obtained here can be robustly defended as depositional ages for the Barra Velha at these depths.

Recognizing that the Barra Velha Fm could span several million years given the absence of absolute ages to bracket this stratigraphy, and that the age uncertainty on the sample from a depth of 37.3 m below the Ariri Fm in well 1 is 4.7 Ma, we suggest that a conservative age for the Barra Velha Fm is 114.5 ± 4.7 Ma. However, the ID age obtained from the sample taken from a depth of 27.6 m below the Ariri Fm in well 3 provides a far more precise age of 115.83 ± 1.56 Ma. We consider this to be a robust age that calibrates the Barra Velha Fm in the Santos Basin. Given that the pre-salt stratigraphy immediately underlying the regional salt sequences yields the same $^{87}Sr/^{86}Sr$ in both the Santos and Campos basins, this age constraint likely extrapolates for the timing of deposition for the Macabu Fm, and potentially the equivalent pre-salt stratigraphy on the West African margin. Furthermore, it provides the first robust maximum age constraint for the overlying evaporites given the uncertainty associated with previously published igneous age determinations (i.e., extrusive ages versus intrusive ages) and the full understanding of the stratigraphic sequences needed to place such ages in to context. Finally, this age challenges the association between the deposition of the regional evaporites and OAE 1a at 120–125 Ma as proposed by Tedeschi et al. (2017). Instead, we suggest that salt deposition occurred in the period between our U-Pb age of Barra Valha Fm deposition of 115.8 Ma and ca. 113 Ma based on the post-salt upper Aptian biostratigraphic constraints from West Africa and Brazil (Kochhann et al., 2013; Sanjinés et al., 2022). Further work is required to develop a more complete age and environmental record of lacustrine carbonate deposition within these basins. However, this study provides a blue-print for how future studies should integrate geochronology and thermometry to understand the temporal and environmental evolution of the South Atlantic during the terminal stages of continental breakup.

CONCLUSIONS

(1) Our integrated petrographic and geochemical study of pre-salt wells from four carbonate platforms in the Santos Basin provides the most robust constraints to date on the age and depositional conditions that prevailed within the Cretaceous pre-salt lakes of the central South Atlantic.

(2) We have constrained the depositional age of the upper Barra Velha Fm to be 115.83 ± 1.56 Ma through isotope dilution U-Pb dating. This age is consistent with overlapping laser ablation U-Pb ages of 114.46 ± 4.72 Ma and 109.73 ± 9.26 Ma from two separate carbonate platforms in the Santos Basin.

(3) Carbonate clumped isotope temperatures of 36 ± 8 °C and and 38 ± 5 °C provide the first direct thermometry constrains on the depositional temperatures of the Barra Velha Fm. Associated carbonate $\delta^{18}O$ values for these samples allow us to calculate the $\delta^{18}O$ of the water in these ancient lakes to be between 1.9 and 4.9‰$_{(VSMOW)}$. These values are consistent with lake waters that have been subject to high levels of evaporation in a relatively arid climate.

(4) The majority of carbonate clumped isotope apparent temperatures measured in this study record temperatures in excess of 40 °C. Through integration with detailed petrographic analysis, we interpret these temperatures to reflect the overprinting of depositional fabrics by various stages of diagenesis. Cooler temperatures are associated with samples that contain the highest fraction of early silica diagenesis, while the hottest temperatures are associated with extensive dolomitization that is shown to be a product of late-stage burial diagenesis.

ACKNOWLEDGMENTS

The authors would like to thank Agência Nacional do Petróleo, Gás Natural e Biocombustíveis for access to samples for this study. We also thank Petrobras for support at their facilities during sampling of the cores and sidewall cores.

REFERENCES CITED

Antonietto, L., Gobbo, S., Do Carmo, D., Assine, M., Fernandes, M., and Silva, J., 2012, Taxonomy, ontogeny and paleoecology of two species of Harbinia TSAO, 1959 (Crustacea, Ostracoda) from the Santana Formation, Lower Cretaceous, northeastern Brazil: Journal of Paleontology, v. 86, no. 4, p. 659–668. https://doi.org/10.1666/11-012R.1

Ariza Ferreira, D.J., Moreira Lupinacci, W., de Andrade Neves, I., Rodrigues Zambrini, J.P., Luiz Ferrari, A., Pierantoni Gamboa, L.A., and Olho Azul, M., 2019, Unsupervised seismic facies classification applied to a presalt carbonate reservoir, Santos Basin, offshore Brazil: AAPG Bulletin, v. 103, p. 997–1012 https://doi.org/10.1306/10261818055.

Baddouh, M., Carroll, A.R., Meyers, S.R., Beard, B.L., and Johnson, C.M., 2017, Chronostratigraphic correlation of lacustrine deposits using $^{87}Sr/^{86}Sr$ ratios, Eocene Green River Formation, Wyoming, U.S.A: Journal of Sedimentary Research, v. 87, p. 406–423, https://doi.org/10.2110/jsr.2017.27.

Bahniuk, A.M., Anjos, S., França, A.B., Matsuda, N., Eiler, J., Mckenzie, J.A., and Vasconcelos, C., 2015, Development of microbial carbonates in the Lower Cretaceous Codó Formation (north-east Brazil): Implications for interpretation of microbialite facies associations and palaeoenvironmental conditions: Sedimentology, v. 62, p. 155–181, https://doi.org/10.1111/sed.12144.

Bate, R.H., 1999, Non-marine ostracod assemblages of the Pre-Salt rift basins of West Africa and their role in sequence stratigraphy, *in* Cameron, N.R., Bate, R.H., and Clure, V.S., eds., The Oil and Gas Habitats of the South Atlantic: Geological Society of London, Special Publications, v. 153, p. 283–292, https://doi.org/10.1144/GSL.SP.1999.153.01.17.

Bonifacie, M., Calmels, D., Eiler, J.M., Horita, J., Chaduteau, C., Vasconcelos, C., Agrinier, P., Katz, A., Passey, B.H., Ferry, J.M., and Bourrand, J.-J., 2017, Calibration of the dolomite clumped isotope thermometer from 25 to 350 °C, and implications for a universal calibration for all (Ca, Mg, Fe)CO_3 carbonates: Geochimica et Cosmochimica Acta, v. 200, p. 255–279, https://doi.org/10.1016/j.gca.2016.11.028.

Cruset, D., Cantarero, I., Trave, A., Verges, J., and John, C.M., 2016, Crestal graben fluid evolution during growth of the Puig-reig anticline (South Pyrenean fold and thrust belt): Journal of Geodynamics, v. 101, p. 30–50, https://doi.org/10.1016/j.jog.2016.05.004.

Davison, I., 2007, Geology and tectonics of the South Atlantic Brazilian salt basins, *in* Ries, A.C., Butler, R.W.H., and Graham, R.H., eds., Deformation of the Continental Crust: The Legacy of Mike Coward: Geological Society of London, Special Publications, v. 272, p. 345–359, https://doi.org/10.1144/GSL.SP.2007.272.01.18.

De Boever, E., Brasier, A.T., Foubert, A., and Kele, S., 2017, What do we really know about early diagenesis of non-marine carbonates?: Sedimentary Geology, v. 361, p. 25–51, https://doi.org/10.1016/j.sedgeo.2017.09.011.

Dennis, K.J., Affek, H.P., Passey, B.H., Schrag, D.P., and Eiler, J.M., 2011, Defining an absolute reference frame for 'clumped' isotope studies of CO_2: Geochimica et Cosmochimica Acta, v. 75, p. 7117–7131, https://doi.org/10.1016/j.gca.2011.09.025.

Devriendt, L.S., Watkins, J.M., and McGregor, H.V., 2017, Oxygen isotope fractionation in the $CaCO_3$-DIC-H_2O system: Geochimica et Cosmochimica Acta, v. 214, p. 115–142, https://doi.org/10.1016/j.gca.2017.06.022.

Dias, J.L., Sad, A.R.E., Fontana, R.L., and Feijo, F.J., 1994, Bacia de Pelotas: Boletim de Geosiencias da Petrobras, v. 8, p. 235–245.

Dickinson, W.R., 1985, Interpreting provenance relations from detrital modes, *in* Zuffa, G.G., ed., Provenance of Arenites: Berlin, Germany, Springer, NATO ASI Series 148, p. 333–361.

Dill, H.G., 2001, The geology of aluminium phosphates and sulphates of the alunite group minerals: A review: Earth-Science Reviews, v. 53, p. 35–93, https://doi.org/10.1016/S0012-8252(00)00035-0.

Farias, F., Szatmari, P., Bahniuk, A., and França, A.B., 2019, Evaporitic carbonates in the pre-salt of Santos Basin – Genesis and tectonic implications: Marine and Petroleum Geology, v. 105, p. 251–272, https://doi.org/10.1016/j.marpetgeo.2019.04.020.

Gamboa, C., Godfrey, L., Herrera, C., Custodio, E., and Soler, A., 2019, The origin of solutes in groundwater in a hyper-arid environment: A chemical and multi-isotope approach in the Atacama Desert, Chile: The Science of the Total Environment, v. 690, p. 329–351, https://doi.org/10.1016/j.scitotenv.2019.06.356.

Ghosh, P., Adkins, J., Affek, H., Balta, B., Guo, W., Schauble, E.A., Schrag, D., and Eiler, J.M., 2006, ^{13}C–^{18}O bonds in carbonate minerals: A new kind of paleothermometer: Geochimica et Cosmochimica Acta, v. 70, p. 1439–1456, https://doi.org/10.1016/j.gca.2005.11.014.

Gomes, J.P., Bunevich, R.B., Tedeschi, L.R., Tucker, M.E., and Whitaker, F.F., 2020, Facies classification and patterns of lacustrine carbonate deposition of the Barra Velha Formation, Santos Basin, Brazilian Pre-salt: Marine and Petroleum Geology, v. 113, https://doi.org/10.1016/j.marpetgeo.2019.104176.

Hart, W.S., Quade, J., Madsen, D.B., Kaufman, D.S., and Oviatt, C.G., 2004, The $^{87}Sr/^{86}Sr$ ratios of lacustrine carbonates and lake-level history of the Bonneville paleolake system: Geological Society of America Bulletin, v. 116, p. 1107–1119, https://doi.org/10.1130/B25330.1.

Horton, T.W., Defliese, W.F., Tripati, A.K., and Oze, C., 2016, Evaporation induced ^{18}O and ^{13}C enrichment in lake systems: A global perspective on hydrologic balance effects: Quaternary Science Reviews, v. 131, p. 365–379, https://doi.org/10.1016/j.quascirev.2015.06.030.

Jones, C.E., and Jenkyns, H.C., 2001, Seawater strontium isotopes, oceanic anoxic events, and seafloor hydrothermal activity in the Jurassic and Cretaceous: American Journal of Science, v. 301, https://doi.org/10.2475/ajs.301.2.112.

Karner, G., Johnson, C., Shoffner, J., Lawson, M., Sullivan, M., Sitgreaves, J., McHarge, J., Stewart, J., and Figueredo, P., 2021, Tectono-magmatic development of the Santos and Campos basins, offshore Brazil, *in* Mello, M.R., Yilmaz, P.O., and Katz, B.J., eds., The supergiant Lower Cretaceous pre-salt petroleum system of the Santos Basin, Brazil: AAPG Memoir 124, p. 215–256.

Kele, S., Breitenbach, S.F.M., Capezzuoli, E., Meckler, A.N., Ziegler, M., Millan, I.M., Kluge, T., Deák, J., Hanselmann, K., John, C.M., Yan, H., Liu, Z., and Bernasconi, S.M., 2015, Temperature dependence of oxygen- and clumped isotope fractionation in carbonates: A study of travertines and tufas in the 6–95°C temperature range: Geochimica et Cosmochimica Acta, v. 168, p. 172–192, https://doi.org/10.1016/j.gca.2015.06.032.

Kim, S.-T., and O'Neil, J.R., 1997, Equilibrium and nonequilibrium oxygen isotope effects in synthetic carbonates: Geochimica et Cosmochimica Acta, v. 61, p. 3461–3475, https://doi.org/10.1016/S0016-7037(97)00169-5.

Kochhann, K.G.D., Koutsoukos, E.A.M., Fauth, G., and Sial, A.N., 2013, Aptian-Albian planktic foraminifera from DSDP site 364 (offshore Angloa): Biostratigraphy, paleoecology, and paleoceanographic significance: Journal of Foraminiferal Research, v. 43, https://doi.org/10.2113/gsjfr.43.4.443.

Lawson, M., Shenton, B.J., Stolper, D.A., Eiler, J.M., Rasbury, E.T., Becker, T.P., Phillips-Lander, C.M., Buono, A.S., Becker, S.P., Pottorf, R., Gray, G.G., Yurewicz, D., and Gournay, J., 2018, Deciphering the diagenetic history of the El Abra Formation of eastern Mexico using reordered clumped isotope temperatures and U-Pb dating: Geological Society of America Bulletin, v. 130, p. 617–629, https://doi.org/10.1130/B31656.1.

Lima, B.E.M., Tedeschi, L.R., Pestilho, A.L.S., Santos, R.V., Vazquez, J.C., Guzzo, J.V.P., and De Ros, L.F., 2020, Deep-burial hydrothermal alteration of the Pre-Salt carbonate reservoirs from northern Campos Basin, offshore Brazil: Evidence from petrography, fluid inclusions, Sr, C and O isotopes: Marine and Petroleum Geology, v. 113, https://doi.org/10.1016/j.marpetgeo.2019.104143.

Ludwig, K.R., 1993, PBDAT: A computer program for processing Pb-U-Th isotope data: U.S. Geological Survey, Open File Report 88-542.

Ludwig, K.R., 2003, User's manual for Isoplot 3.00: A geochronological toolkit for Microsoft Excel: Berkeley Geochronology Center Special Publication, v. 4, 70 p.

McArthur, J.M., Howarth, R.J., and Bailey, T.R., 2001, Strontium Isotope Stratigraphy: LOWESS Version 3: Best Fit to the Marine Sr-Isotope Curve for 0–509 Ma and Accompanying Look-up Table for Deriving Numerical Age: The Journal of Geology, v. 109, p. 155–170, https://doi.org/10.1086/319243.

Moreira, J.L.P., Madeira, C.V., Gil, J.A., and Machado, M.A.P., 2007, Bacia de Santos: Boletim de Geosiencias da Petrobras, v. 15, p. 531–549.

Parrish, J.T., Rasbury, E.T., Chan, M.A., and Hasiotis, S.T., 2019, Earliest Jurassic U-Pb ages from carbonate deposits in the Navajo Sandstone, southeastern Utah, USA: Geology, v. 47, p. 1015–1019, https://doi.org/10.1130/G46338.1.

Passey, B.H., and Henkes, G.A., 2012, Carbonate clumped isotope bond reordering and geospeedometry: Earth and Planetary Science Letters, v. 351–352, p. 223–236, https://doi.org/10.1016/j.epsl.2012.07.021.

Passey, B.H., Levin, N.E., Cerling, T.E., Brown, F.H., and Eiler, J.M., 2010, High-temperature environments of human evolution in East Africa based on bond ordering in paleosol carbonates: Proceedings of the National Academy of Sciences of the United States of America, v. 107, p. 11245–11249, https://doi.org/10.1073/pnas.1001824107.

Paton, C., Hellstrom, J., Paul, B., Woodhead, J., and Hergt, J., 2011, Iolite: Freeware for the visualisation and processing of mass spectrometric data: Journal of Analytical Atomic Spectrometry, v. 26, p. 2508–2518, https://doi.org/10.1039/c1ja10172b.

Pietzsch, R., 2021, Comment on "Evaporitic carbonates in the pre-salt of Santos Basin – Genesis and tectonic implications": Marine and Petroleum Geology, v. 133, https://doi.org/10.1016/j.marpetgeo.2021.104963.

Pietzsch, R., Oliveira, D.M., Tedeschi, L.R., Queiroz Neto, J.V., Figueiredo, M.F., Vazquez, J.C., and de Souza, R.S., 2018, Palaeohydrology of the Lower Cretaceous pre-salt lacustrine system, from rift to post-rift phase, Santos Basin, Brazil: Palaeogeography, Palaeoclimatology, Palaeoecology, v. 507, p. 60–80, https://doi.org/10.1016/j.palaeo.2018.06.043.

Pietzsch, R., Tedeschi, L.R., Oliveira, D.M., dos Anjos, C.W.D., Vazquez, J.C., and Figueiredo, M.F., 2020, Environmental conditions of deposition of the Lower Cretaceous lacustrine carbonates of the Barra Velha Formation, Santos Basin (Brazil), based on stable carbon and oxygen isotopes: A continental record of pCO2 during the onset of the Oceanic Anoxic Event 1a (OAE 1a) interval?: Chemical Geology, v. 535, https://doi.org/10.1016/j.chemgeo.2019.119457.

Poropat, S.F., and Colin, J.-P., 2012a, Early Cretaceous ostracod biostratigraphy of eastern Brazil and western Africa: An overview: Gondwana Research, v. 22, p. 772–798, https://doi.org/10.1016/j.gr.2012.06.002.

Poropat, S.F., and Colin, J.-P., 2012b, Reassessment of the Early Cretaceous non-marine ostracod genera *Hourcqia* Krömmelbein, 1965 and *Pattersoncypris* Bate, 1972 with the description of a new genus, *Kroemmelbeincypris*: Journal of Paleontology, v. 86, p. 699–719, https://doi.org/10.1666/11-140R.1.

Rangel, H.D., Martins, F.A.L., Esteves, F.R., and Feijo, F.J., 1994, Bacia de Campos: Boletim de Geosiencias da Petrobras, v. 8, p. 203–217.

Roberts, N.M.W., Rasbury, E.T., Parrish, R.R., Smith, C.J., Horstwood, M.S.A., and Condon, D.J., 2017, A calcite reference material for LA-ICP-MS U-Pb geochronology: Calcite RM for LA-ICP-MS U-Pb dating: Geochemistry, Geophysics, Geosystems, v. 18, p. 2807–2814, https://doi.org/10.1002/2016GC006784.

Rodriguez, C.R., Jackson, C.A.-L., Rotevatn, A., Bell, R.E., and Francis, M., 2018, Dual tectonic-climatic controls on salt giant deposition in the Santos Basin, offshore Brazil: Geosphere, v. 14, p. 215–242, https://doi.org/10.1130/GES01434.1.

Saller, A., Rushton, S., Buambua, L., Inman, K., McNeil, R., Dickson, J.A.D., 2016, Presalt stratigraphy and depositional systems in the Kwanza Basin, offshore Angola: AAPG Bulletin, v. 100, p. 1135–1164, https://doi.org/10.1306/02111615216.

Sanjinés, A.E.S., Viviers, M.C., Costa, D.S., Zerfass, G.S.A., Beurlen, G., and Strohschoen, O., 2022, Planktonic foraminifera from the Aptian section of the southeastern Brazilian Atlantic margin: Cretaceous Research, v. 134, https://doi.org/10.1016/j.cretres.2022.105141.

Shenton, B.J., Grossman, E.L., Passey, B.H., Henkes, G.A., Becker, T.P., Laya, J.C., Perez-Huerta, A., Becker, S.P., and Lawson, M., 2015, Clumped isotope thermometry in deeply buried sedimentary carbonates: The effects of bond reordering and recrystallization: Geological Society of America Bulletin, v. 127, p. 1036–1051, https://doi.org/10.1130/B31169.1.

Stolper, D.A., and Eiler, J.M., 2015, The kinetics of solid-state isotope-exchange reactions for clumped isotopes: A study of inorganic calcites and apatites from natural and experimental samples: American Journal of Science, v. 315, p. 363–411, https://doi.org/10.2475/05.2015.01.

Szatmari, P., de Lima, C.M., Fontaneta, G., Lima, N. de M., Zambonato, E., Menezes, M.R., Bahniuk, J., Coelho, S.L., Figueiredo, M., Florencio, C.P., and Gontijo, R., 2021, Petrography, geochemistry and origin of South Atlantic evaporites: The Brazilian side: Marine and Petroleum Geology, v. 127, https://doi.org/10.1016/j.marpetgeo.2020.104805.

Tedeschi, L.R., Jenkyns, H.C., Robinson, S.A., Sanjinés, A.E.S., Viviers, M.C., Quintaes, C.M.S.P., and Vazquez, J.C., 2017, New age constraints on Aptian evaporites and carbonates from the South Atlantic: Implications for Oceanic Anoxic Event 1a: Geology, v. 45, p. 543–546, https://doi.org/10.1130/G38886.1.

Vermeesch, P., 2018, IsoplotR: A free and open toolbox for geochronology: Geoscience Frontiers, v. 9, p. 1479–1493, https://doi.org/10.1016/j.gsf.2018.04.001.

Watkins, J.M., and Hunt, J.D., 2015, A process-based model for non-equilibrium clumped isotope effects in carbonates: Earth and Planetary Science Letters, v. 432, p. 152–165, https://doi.org/10.1016/j.epsl.2015.09.042.

Wright, V.P., 2022, The mantle, CO_2 and the giant Aptian chemogenic lacustrine carbonate factory of the South Atlantic: Some carbonates are made, not born: Sedimentology, v. 69, p. 47–73, https://doi.org/10.1111/sed.12835.

Wright, V.P., and Barnett, A.J., 2015, An abiotic model for the development of textures in some South Atlantic early Cretaceous lacustrine carbonates, *in* Bosence, D.W.J., Gibbons, K.A., Le Heron, D.P., Morgan, W.A., Pritchard, T., and Vining, B.A., eds., Microbial Carbonates in Space and Time: Implications for Global Exploration and Production: Geological Society of London, Special Publications, v. 418, p. 209–219, https://doi.org/10.1144/SP418.3.

Wright, V.P., and Barnett, A.J., 2020, The textural evolution and ghost matrices of the Cretaceous Barra Velha Formation carbonates from the Santos Basin, offshore Brazil: Facies, v. 66, no. 7, https://doi.org/10.1007/s10347-019-0591-2.

Zuffa, G.G., 1980, Hybrid arenites: Their composition and classifications: Journal of Sedimentary Petrology, v. 50, p. 21–29.

Science Editor: Brad S. Singer
Associate Editor: Alan Rooney

Manuscript Received 25 October 2021
Revised Manuscript Received 11 February 2022
Manuscript Accepted 7 April 2022

Printed in the USA